Improving Amide Proton Transfer-weighted MRI Reconstruction using T2-weighted Images

Puyang Wang[1], Pengfei Guo[2], Jianhua Lu[3],
Jinyuan Zhou[3], Shanshan Jiang[3], Vishal M. Patel[1,2]

[1] Department of Electrical and Computer Engineering, Johns Hopkins University, MD, USA
[2] Department of Computer Science, Johns Hopkins University, MD, USA
[3] Department of Radiology, Johns Hopkins University, Baltimore, MD, USA
pwang47@jhu.edu

Abstract. Current protocol of Amide Proton Transfer-weighted (APTw) imaging commonly starts with the acquisition of high-resolution T2-weighted (T_2w) images followed by APTw imaging at particular geometry and locations (i.e. slice) determined by the acquired T_2w images. Although many advanced MRI reconstruction methods have been proposed to accelerate MRI, existing methods for APTw MRI lacks the capability of taking advantage of structural information in the acquired T_2w images for reconstruction. In this paper, we present a novel APTw image reconstruction framework that can accelerate APTw imaging by reconstructing APTw images directly from highly undersampled k-space data and corresponding T_2w image at the same location. The proposed framework starts with a novel sparse representation-based slice matching algorithm that aims to find the matched T_2w slice given only the undersampled APTw image. A Recurrent Feature Sharing Reconstruction network (RFS-Rec) is designed to utilize intermediate features extracted from the matched T_2w image by a Convolutional Recurrent Neural Network (CRNN), so that the missing structural information can be incorporated into the undersampled APT raw image thus effectively improving the image quality of the reconstructed APTw image. We evaluate the proposed method on two real datasets consisting of brain data from rats and humans. Extensive experiments demonstrate that the proposed RFS-Rec approach can outperform the state-of-the-art methods.

Keywords: Magnetic Resonance Imaging · Image Reconstruction · Amide Proton Transfer Imaging

1 Introduction

Amide Proton Transfer-weighted (APTw) imaging is an emerging molecular Magnetic Resonance Imaging (MRI) method that can generate image contrast unique from the conventional MRI. As a type of chemical exchange saturation transfer (CEST) MRI, APTw signal intensity is based on concentrations of endogenous mobile proteins and peptides or tissue pH. Moreover, APTw MRI does

not require any contrast agent administration. Previous studies in animals and humans have demonstrated that APT imaging is capable of detecting brain tumors [18] and ischemic stroke [10]. In a recent preclinical study [11], APT imaging was shown to accurately detect intracerebral hemorrhage and distinctly differentiate hyperacute hemorrhage from cerebral ischemia. Notably, the capability and uniqueness of APT imaging for the detection of primary and secondary brain injuries in experimental Controlled Cortical Impact (CCI) Traumatic Brain Injury (TBI) models have recently been explored with promising results [14].

However, relatively long acquisition times due to the use of multiple RF saturation frequencies and multiple acquisitions to increase the signal-to-noise ratio (SNR) hinders the wide spread clinical use of APTw imaging. A typical CEST MRI acquisition currently requires long scan times in the range of 5 to 10 minutes. Recently, several methods have been developed to accelerate CEST/APT acquisitions. These can be classified into conventional fast imaging techniques (e.g. turbospin-echo [17]) and reduced k-space acquisition techniques (including spectroscopy with linear algebraic modeling [15] and compressed sensing (CS) [3]) that require more advanced data processing. Due to recent advances in deep learning, deep learning-based methods have shown to provide much better generic MRI image reconstruction results from undersampled k-space data than conventional CS-based methods. The combination of convolutional autoencoder and generative adversarial networks can perform faster and more accurate reconstruction [7]. In [12], a pyramid convolutional Recurrent Neural Network (RNN) was designed to iteratively refine reconstructed image in three different feature scales.

Despite the success of deep learning-based MR image reconstruction methods for single contrast/modality imaging, multi-contrast reconstruction still remains a challenge. In multiple-contrast MR imaging it is beneficial to utilize fully sampled images acquired at one contrast for the reconstruction of undersampled MR images in another contrast [4]. For instance, information pertaining to undersampled T_1w images and undersampled T_2w images can be mutually beneficial when reconstructing both images. A joint reconstruction network of T_1, T_2 and PD images was proposed in [9] and was shown to outperform single-contrast models. Furthermore, undersampled T_2w image scan be reconstructed more accurately using the information from fully sampled high-resolution T_1w images [2]. To this end, Y-net was proposed in [2] by modifying U-net which takes two inputs and produces a single output. Features extracted from two independent encoders are concatenated together to generate the final output reconstruction. However, these methods are only evaluated on structural MR images and can be affected by slice mismatch between different scans. To deal with this issue, additional registration process between the images might be required.

Current 2D APTw imaging protocol starts with a high-resolution 3D T_2w scan that is used to locate the slice of interest (usually contains lesion region) by examination. After setting the interested slice, to reduce the effect of B_0 field inhomogeneity on APT imaging, high-order localized slab shimming is performed around the lesion. The final APTw image is defined as the difference of ± 3.5
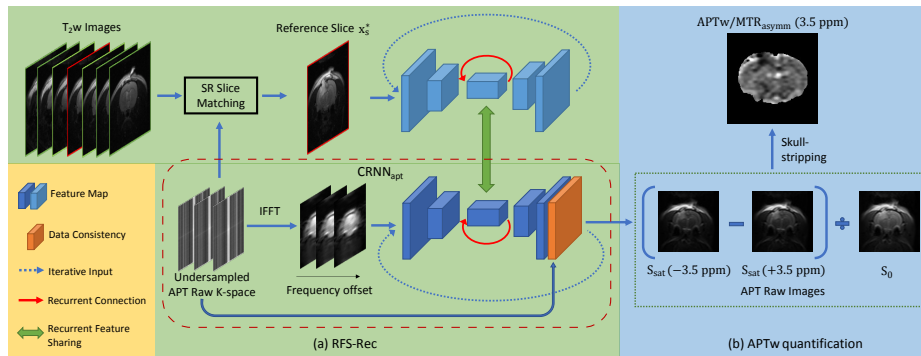
Fig. 1. An overview of the proposed framework.

ppm image normalized by unsaturated image. While one can accelerate APTw imaging by reducing the raw k-space measurement data and apply reconstruction using off-the-shelf algorithms, no existing methods take 3D T_2w scan into reconstruction process as the idea of multi-contrast MR reconstruction suggests.

In this paper, in order to leverage the structural information of T_2w images, we present a Recurrent Feature Sharing Reconstruction network (RFS-Rec) that has two convolutional RNNs (CRNN). These two CRNNs are connected by the proposed recurrent feature sharing approach to encourage bi-directional flow of information. In addition, we propose a sparse representation-based slice matching algorithm to find the corresponding slice in T_2w volume given the undersampled APT k-space data. As a result, input T_2w and APT raw images are aligned and mutual information can be maximized.

2   Methodology

In this section, we first give a brief introduction of APTw imaging. Then we describe our recurrent feature sharing reconstruction network and sparse representation (SR) based slice matching algorithm. As shown in Fig.1, the slice matching step in the proposed framework takes T_2w images and undersampled k-space as input and selects out a reference T_2w slice. The APT raw images are reconstructed by RFS-Rec using both reference T_2w slice and undersampled APT k-space data.

2.1   APTw Imaging

CEST effects are usually analyzed using Z-spectrum, in which the intensity of the water signal during saturation at a frequency offset from water, $S_{\text{sat}}(\Delta\omega)$, normalized by the signal without saturation S_0, is displayed as a function of irradiation frequency using the water frequency as a zero-frequency reference. The sum of all saturation effects at a certain offset is called the magnetization transfer ratio (MTR), defined as follows

$$MTR(\Delta\omega) = 1 - Z(\Delta\omega) = 1 - \frac{S_{\text{sat}}(\Delta\omega)}{S_0}, \tag{1}$$
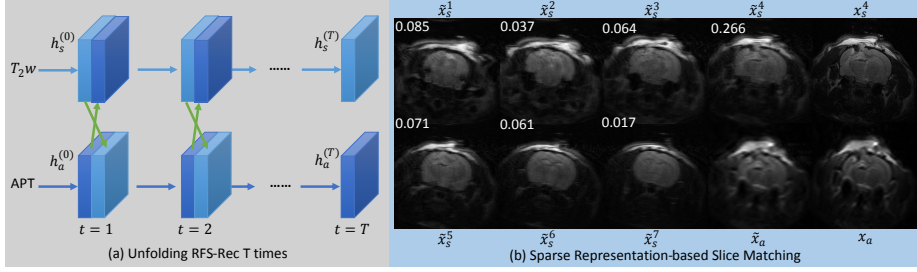
Fig. 2. (a) The proposed recurrent neural network, RFS-Rec, can be unfolded T times. Hidden states of T$_2$w and APT RNN are connected by two-way feature sharing. (b) Absolute weights in sparse vector w_a are shown at the top left corner of the corresponding T$_2$w slices. x_a is the average of fully sampled APT raw images.

where $Z = S_{\text{sat}}/S_0$ is the signal intensity in the Z-spectrum. As a type of CEST, APTw imaging is designed to detect the exchangeable amide protons in the backbone of mobile proteins and are assessed using magnetization transfer ratio asymmetry at 3.5ppm, namely $MTR_{\text{asymm}}(3.5\text{ppm})$ as APTw signal

$$
\begin{aligned}
APTw &= MTR_{\text{asymm}}(3.5\text{ppm}) \\
&= MTR(+3.5\text{ppm}) - MTR(-3.5\text{ppm}) \\
&= \frac{S_{\text{sat}}(-3.5\text{ppm}) - S_{\text{sat}}(+3.5\text{ppm})}{S_0}.
\end{aligned}
\tag{2}
$$

Hence, the quality of APTw image solely depends on the above three images at different frequency offsets. An example of APTw quantification is shown in the right part of Fig. 1. For visualization purpose, skull-stripping procedure is usually performed on APTw image. In the rest of paper, we refer $S_{\text{sat}}(\pm 3.5\text{ppm})$ and S_0 as APT raw images and $MTR_{\text{asymm}}(3.5\text{ppm})$ as an APTw image.

2.2   Recurrent Feature Sharing Reconstruction

The data acquisition process of accelerated MRI can be formulated as follows

$$
y = F_D x + \epsilon ,
\tag{3}
$$

where $x \in \mathbb{C}^M$ is the fully sampled image, $y \in \mathbb{C}^N$ is the observed k-space, and ϵ is the noise. Both x and y are image data represented in vector forms. F_D is the undersampling Fourier encoding matrix which is defined as the multiplication of the Fourier transform matrix F and the binary undersampling matrix D. We define the acceleration factor R as the ratio of the amount of k-space data required for a fully sampled image to the amount collected in an accelerated acquisition. The goal of MRI image reconstruction is to estimate image x from the observed k-space y. MRI reconstruction problem is an ill-posed problem due to the information loss in the forward process as $N \ll M$.

We solve the MRI image reconstruction problem in an iterative manner using CRNN as the base reconstruction network in RFS-Rec. A single contrast CRNN can be divided into four parts: 1) encoder f_{enc}, 2) decoder f_{dec}, 3) hidden state transition f_{res} consisting of two residual convolution blocks (ResBlock), and 4) data consistency (DC) layer. f_{enc} and f_{dec} are constructed using strided and

transposed convolutions. Input images to CRNN are zero-filled undersampled complex APT raw images $x^{(0)} = F_D^H y$ with real and imaginary values as two channels. The output of the $(t+1)^{th}$ iteration of a single CRNN_{apt} model can be described as follows:

$$x^{(t+1)} = \text{DC}(f(x^{(t)}, h^{(t)}, y, D)),$$
$$= F^{-1}[Dy + (1-D)Ff_{dec}(f_{res}(h^{(t)}) + f_{enc}(x^{(t)}))], \quad (4)$$

where $h^{(t)} = f_{res}(h^{(t-1)}) + f_{enc}(x^{(t-1)})$ is the hidden state from the previous iteration and $h^{(0)} = 0$.

As discussed above, by using the information from other contrast, one can more accurately reconstruct an image of another contrast. This approach is known as multi-contrast MRI reconstruction [1]. Information or feature sharing has been shown to be the key for multi-contrast MR image reconstruction [2][9].

Note that CRNNs have been proposed for MRI reconstruction [6] and it has been demonstrated that they can outperform cascaded models and U-net [8]. However, feature sharing in CRNN has not been studied in the literature for MRI reconstruction. In this paper, we present a novel recurrent feature sharing method that exchanges intermediate hidden state features of two CRNNs (see Fig.2(a)). This allows us to use CRNNs for multi-contrast MR image reconstruction in a more efficient way.

The proposed RFS-Rec consists of two CRNNs, CRNN_{apt} and CRNN_{t2w}. CRNN_{t2w} for T_2w images are constructed similar to CRNN_{apt} which is defined in Eq.4 but without the DC layer. CRNN_{t2w} takes the reference slice x_s^* which is assumed to be aligned with underlying full sampled x.

To enable two-way information flow between APT features h_a and structural T_2w features h_s, we add bi-directional skip connection links (Fig.2(a)) in each iteration, which is inspired by the one-time feature concatenation in Y-net [2]. Thus, the overall dynamics of our proposed RFS-Rec is given as follows

$$h_a^{(t)} = f_{res}(h_a^{(t-1)} \oplus h_s^{(t-1)}) + f_{enc}(x^{(t-1)}), \text{ and}$$
$$h_s^{(t)} = f_{res}(h_s^{(t-1)} \oplus h_a^{(t-1)}) + f_{enc}(x_s^{(t-1)}), \quad (5)$$

where $\oplus$ stands for channel-wise concatenation. We refer to this hidden state exchange design as recurrent feature sharing.

In terms of the loss function, we use a combination of the Normalised Mean Square Error (NMSE) loss and the Structural Similarity Index (SSIM) loss as our training loss. The overall loss function we use to train the network is defined as follows

$$\mathcal{L}(\hat{x}, x) = \mathcal{L}_{\text{NMSE}} + \beta\mathcal{L}_{\text{SSIM}},$$
$$= \frac{\|\hat{x} - x\|_2^2}{\|x\|_2^2} + \beta\frac{(2\mu_{\hat{x}}\mu_x + c_1)(2\sigma_{\hat{x}x} + c_2)}{(\mu_{\hat{x}}^2 + \mu_x^2 + c_1)(\sigma_{\hat{x}}^2 + \sigma_x^2 + c_2)}, \quad (6)$$

where $\mu_{\hat{x}}$ and μ_x are the average pixel intensities in $\hat{x}$ and x, respectively, $\sigma_{\hat{x}}^2$ and σ_x^2 are their variances, $\sigma_{\hat{x}x}$ is the covariance between $\hat{x}$ and x, and $c_1 = (k_1 L)^2$, $c_2 = (k_2 L)^2$. In this paper, we choose a window size of 7×7, and set $k_1 = 0.01$, $k_2 = 0.03$, and define L as the maximum magnitude value of the target image x, i.e. $L = \max(|x|)$. We use $\beta = 0.5$ to balance the two loss functions.

2.3   Sparse Representation-based Slice Matching

As mentioned earlier, a 3D T_2w scan is normally acquired prior to 2D APTw imaging. In order to fully leverage the T_2w scan, it is important to identify the matching slices between T_2w and the undersampled APT raw image. We propose a simple yet effective sparse representation-based slice matching algorithm that can find the closest slice in T_2w scan in terms of location given undersampled APT raw images.

Sparse representation-based approach, first described in [13], exploits the discriminative nature of sparsity. The average undersampled APT raw image can be represented by a set of T_2w images as a linear combination of all elements. This representation is naturally sparse and can be recovered efficiently via ℓ_1-minimization, seeking the sparsest representation of the APT raw image. Let $X_s = [\tilde{x}_s^1, \ \tilde{x}_s^2, \ldots, \ \tilde{x}_s^n]$ be the matrix that contains all n undersampled structural T_2w slices, $\tilde{x}_s = F_D^H F_D x_s$ and $\tilde{x}_a = \sum_{i=1}^{3} F_D^H y_i / 3$ be the average of the undersampled APT raw images. The sparsest vector w_a that represents $\tilde{x}_a$ in X_s and gives small reconstruction error $\|\tilde{x}_a - X_s w_a\|_2$ can be found by solving the following l_1-minimization problem

$$w_a = \underset{w}{\operatorname{argmin}} \|w\|_1 \quad \text{s.t.} \quad \|\tilde{x}_a - X_s w\|_2 \leq \sigma. \tag{7}$$

After solving the optimization problem, the matching T_2w slice x_s^* is determined by the slice index $i = \operatorname{argmax} |w_a^i|$ (i.e. the slice with the largest absolute weight). From an example of SR slice matching ($\sigma = 0.1$) shown in Fig.2(b), x_s^4 which has the largest absolute weight $w_a^4 = 0.266$ is the one matched to the APT raw image $\tilde{x}_a$ and will be used as the reference T_2w image in the reconstruction phase.

3   Experiments

Datasets We evaluate the proposed image reconstruction framework on two datasets.

Rat TBI Data: 300 MRI scans are performed on 65 open-skull rats with controlled cortical impact model of TBI at different time point after TBI. Each MRI scan includes high-resolution T_2w imaging with a fast spin echo sequence in coronal plane (number of slices= 7; matrix= 256×256; field of view (FOV) = 32×32 mm^2; slice thickness = 1.5 mm) and 2D APT (frequency labeling offsets of ±3.5 ppm; matrix= 64×64; FOV = 32×32 mm^2; single slice; slice thickness = 1.5 mm). An unsaturated image S_0 in the absence of radio-frequency saturation was also acquired for APT imaging signal intensity normalization.

Human Brain Tumor Data: 144 3D T_2w and APTw MRI volumes were collected from 90 patients with pathologically proven primary malignant glioma. Imaging parameters for APTw can be summarized as follows: FOV = 212×212×66 mm3; resolution = 0.82×0.82×4.4 mm^3; size in voxel = 256×256×15. T_2w sequences were acquired with the following imaging parameters: FOV = 212×212× 165 mm3; resolution, 0.41×0.41×1.1 mm3 ; size in voxel, 512×512×150. Co-registration between APTw and T_2w sequences[16], and MRI standardization[5]

Table 1. Quantitative results of APT raw image reconstruction under the acceleration factors $R = 4$ and $R = 8$. T_2w indicates whether T_2w image is used during reconstruction. SM denotes the use of the proposed SR slice matching instead of always using the center T_2w slice. Note that, for Human brain dataset, the slice matching does not apply because T_2w and APT volume are already well co-registered.

| Dataset	Method	T_2w	SM	R=4 NMSE	R=4 PSNR	R=4 SSIM	R=8 NMSE	R=8 PSNR	R=8 SSIM
Rat	U-net[8]			0.144	34.29	0.920	0.242	31.96	0.878
	Y-net[2]	✓		0.111	35.35	0.932	0.218	32.29	0.889
	$CRNN_{apt}$			0.087	36.41	0.939	0.217	32.31	0.889
	CRNN	✓		0.085	36.43	0.940	0.219	32.28	0.893
	CRNN	✓	✓	0.084	36.56	0.941	0.212	32.37	0.893
	RFS-Rec	✓	✓	**0.076**	**36.94**	**0.950**	**0.187**	**33.11**	**0.906**
Human	U-net[8]		N/A	0.022	37.19	0.910	0.045	33.76	0.872
	Y-net[2]	✓	N/A	0.014	39.27	0.938	0.037	34.65	0.889
	$CRNN_{apt}$		N/A	0.014	39.64	0.943	0.041	34.30	0.887
	CRNN	✓	N/A	0.012	40.35	0.950	0.038	34.84	0.896
	RFS-Rec	✓	N/A	**0.010**	**40.99**	**0.956**	**0.034**	**35.27**	**0.903**
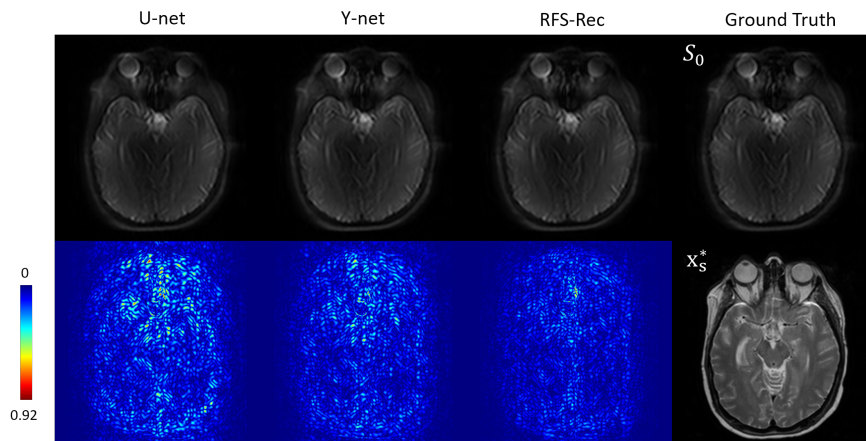
Fig. 3. S_0 reconstructions at $R = 4$ and the corresponding error maps.

were performed. After preprocessing, the final volume size of each sequence is $256 \times 256 \times 15$. Data collection and processing are approved by the Institutional Review Board.

Training Details: We simulated undersampled k-space measurements of APT raw images using the Cartesian sampling method with a fixed 0.08% center frequency sampled and random sampling in other frequencies uniformly. Training and testing subsets are randomly selected with 80/20% split. We conducted model training under the acceleration factors R=4 and 8. All models are implemented in Pytorch and trained on NVIDIA GPUs. Hyperparameters are set as follows: learning rate of 10^{-3} with decreasing rate of 0.9 for every 5 epochs, 60 maximum epochs, batch size of 6. Adam optimizer is used in training all the networks. For CRNN and RFS-Rec, the number of iterations T is set equal to 7.

We compare our proposed RFS-Rec against U-net [8], Y-net [2], single contrast CRNN $_{apt}$, CRNN with concatenation of center T_2w slice and undersam-

(a) Reconstructed APTw image   (a) Error map of reconstructed APTw image
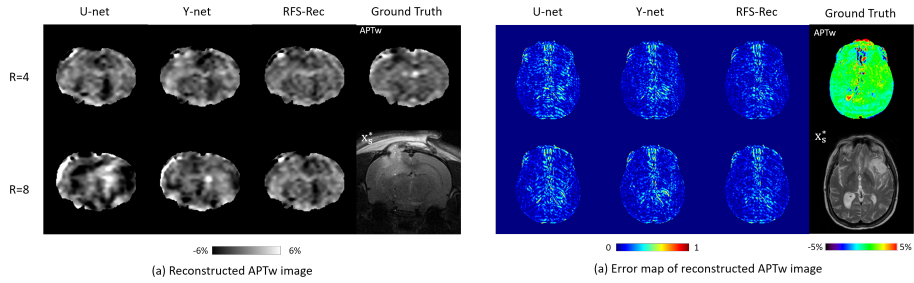
Fig. 4. Results of APTw images derived from the reconstructed APT raw images using Eq.2. Skull-stripping is performed for better visualization. Reference T_2w slice x_s^* used for reconstruction are also shown.

pled APT raw images as input and CRNN using the proposed SR slice matching to select the reference slice. Regarding the U-net implementation, a DC layer was added at the end of the network. The quantitative metrics, including NMSE, PSNR and SSIM, are computed between fully sampled APT raw images ($S_{sat}(\pm 3.5ppm)$ and S_0) and their reconstructions. Detailed quantitative experimental results are shown in Tab.1. It can be seen from the table that the proposed RFS-Rec approach outperforms all the other compared methods on both datasets. Furthermore, the individual contribution of the modules in the proposed method (SR-based slice matching and RFS), are demonstrated by an ablation study (i.e. CRNN with/without SM and RFS-Rec). One interesting observation from Tab. 1 is that the difference between $CRNN_{apt}$ and Y-net, when $R = 8$, on the human dataset is inverse of what we observe on the rat dataset. This may be caused by the good registration of T_2w and APT in the human dataset. The issue of shape inconsistency of the APT raw image and T_2w image in the rat dataset can also be observed by comparing $CRNN_{apt}$ and CRNN with T_2w.

Results of reconstructed S_0 and APTw images compared to the ground truth in Fig.3 and Fig.4 show consistent findings as quantitative results suggest. Our method yields not only better $S_{sat}(\pm 3.5ppm)$ and S_0 reconstruction but also more accurate APTw images.

4   Conclusion

We proposed an APTw image reconstruction network RFS-Rec for accelerating APTw imaging, which can more accurately reconstruct APT raw images by using the information of fully sampled T_2w images. We achieved this goal by incorporating a novel recurrent feature sharing mechanism into two CRNNs which enable two-way information flow between APT and T_2w features. In addition, to maximize the effectiveness of RFS-Rec, we use a sparse representation-based slice matching algorithm to locate reference T_2w slice. Extensive experiments on two real datasets consisting of brain data from rats and humans showed the significance of the proposed work.

References

1. Bilgic, B., Goyal, V.K., Adalsteinsson, E.: Multi-contrast reconstruction with bayesian compressed sensing. Magnetic resonance in medicine **66**(6), 1601–1615 (2011)
2. Do, W.J., Seo, S., Han, Y., Ye, J.C., Hong Choi, S., Park, S.H.: Reconstruction of multi-contrast mr images through deep learning. Medical Physics (2019)
3. Heo, H.Y., Zhang, Y., Lee, D.H., Jiang, S., Zhao, X., Zhou, J.: Accelerating chemical exchange saturation transfer (cest) mri by combining compressed sensing and sensitivity encoding techniques. Magnetic resonance in medicine **77**(2), 779–786 (2017)
4. Huang, J., Chen, C., Axel, L.: Fast multi-contrast mri reconstruction. Magnetic resonance imaging **32**(10), 1344–1352 (2014)
5. Nyúl, L.G., Udupa, J.K., Zhang, X.: New variants of a method of mri scale standardization. IEEE transactions on medical imaging **19**(2), 143–150 (2000)
6. Qin, C., Schlemper, J., Caballero, J., Price, A.N., Hajnal, J.V., Rueckert, D.: Convolutional recurrent neural networks for dynamic mr image reconstruction. IEEE transactions on medical imaging **38**(1), 280–290 (2018)
7. Quan, T.M., Nguyen-Duc, T., Jeong, W.K.: Compressed sensing mri reconstruction using a generative adversarial network with a cyclic loss. IEEE transactions on medical imaging **37**(6), 1488–1497 (2018)
8. Ronneberger, O., Fischer, P., Brox, T.: U-net: Convolutional networks for biomedical image segmentation. In: International Conference on Medical image computing and computer-assisted intervention. pp. 234–241. Springer (2015)
9. Sun, L., Fan, Z., Fu, X., Huang, Y., Ding, X., Paisley, J.: A deep information sharing network for multi-contrast compressed sensing mri reconstruction. IEEE Transactions on Image Processing **28**(12), 6141–6153 (2019)
10. Sun, P.Z., Cheung, J.S., Wang, E., Lo, E.H.: Association between ph-weighted endogenous amide proton chemical exchange saturation transfer mri and tissue lactic acidosis during acute ischemic stroke. Journal of Cerebral Blood Flow & Metabolism **31**(8), 1743–1750 (2011)
11. Wang, M., Hong, X., Chang, C.F., Li, Q., Ma, B., Zhang, H., Xiang, S., Heo, H.Y., Zhang, Y., Lee, D.H., et al.: Simultaneous detection and separation of hyperacute intracerebral hemorrhage and cerebral ischemia using amide proton transfer mri. Magnetic resonance in medicine **74**(1), 42–50 (2015)
12. Wang, P., Chen, E.Z., Chen, T., Patel, V.M., Sun, S.: Pyramid convolutional rnn for mri reconstruction. arXiv preprint arXiv:1912.00543 (2019)
13. Wright, J., Yang, A.Y., Ganesh, A., Sastry, S.S., Ma, Y.: Robust face recognition via sparse representation. IEEE transactions on pattern analysis and machine intelligence **31**(2), 210–227 (2008)
14. Zhang, H., Wang, W., Jiang, S., Zhang, Y., Heo, H.Y., Wang, X., Peng, Y., Wang, J., Zhou, J.: Amide proton transfer-weighted mri detection of traumatic brain injury in rats. Journal of Cerebral Blood Flow & Metabolism **37**(10), 3422–3432 (2017)
15. Zhang, Y., Heo, H.Y., Jiang, S., Lee, D.H., Bottomley, P.A., Zhou, J.: Highly accelerated chemical exchange saturation transfer (cest) measurements with linear algebraic modeling. Magnetic resonance in medicine **76**(1), 136–144 (2016)

16. Zhang, Y., Heo, H.Y., Lee, D.H., Zhao, X., Jiang, S., Zhang, K., Li, H., Zhou, J.: Selecting the reference image for registration of cest series. Journal of Magnetic Resonance Imaging **43**(3), 756–761 (2016)
17. Zhao, X., Wen, Z., Zhang, G., Huang, F., Lu, S., Wang, X., Hu, S., Chen, M., Zhou, J.: Three-dimensional turbo-spin-echo amide proton transfer mr imaging at 3-tesla and its application to high-grade human brain tumors. Molecular imaging and biology **15**(1), 114–122 (2013)
18. Zhou, J., Tryggestad, E., Wen, Z., Lal, B., Zhou, T., Grossman, R., Wang, S., Yan, K., Fu, D.X., Ford, E., et al.: Differentiation between glioma and radiation necrosis using molecular magnetic resonance imaging of endogenous proteins and peptides. Nature medicine **17**(1), 130–134 (2011)